POLITECNICO
MILANO 1863

SCUOLA DI INGEGNERIA INDUSTRIALE
E DELL'INFORMAZIONE

EXECUTIVE SUMMARY OF THE THESIS

Work-related musculoskeletal disorders: passive upper-limbs exoskeleton evaluation and markerless motion capture system validation

TESI MAGISTRALE IN BIOMEDICAL ENGINEERING – INGEGNERIA BIOMEDICA

AUTHOR: SARA BORGHI

ADVISOR: MANUELA GALLI

CO-ADVISOR: FILIPPO MOTTA & GIORGIA PALOTTI

ACADEMIC YEAR: 2025-2026

1. Introduction

Musculoskeletal disorders are defined as structural impairments affecting muscles, joints, tendons and other body components. When these disorders are predominantly induced by occupational activities during work tasks, they are classified as work-related musculoskeletal disorders (WMSDs). They are major cause of concern due to their profound impact not only on workers' health and well-being, but also on economy and financial situation of companies. Decrease in work productivity, absence from work and increase in social health expenses are factors to be considered during a financial report [1]. Furthermore, WMSDs are related to different risk factors that change depending on the task and the working sector. Primarily, awkward non-neutral and extreme postures, repetitive motions performed at high frequency or over prolongated period, not enough time rest and a combination of these factors are prominent components of risk factors [2]. A risk factor analysis is required to identify the main issues in each task and to define a preventive procedure. Among the different strategies used to reduce WMSDs developments, assistive tools, like exoskeletons designed to support the musculoskeletal system, are widely analyzed in literature. Among the different types of exoskeletons applied in WMSDs field, active ones are mainly used for high force exertion during a task, while passive devices are preferrable for the maintenance of static postures and highly repetitive low weight task [3]. This study aims to validate a passive upper limb exoskeleton used during repetitive overhead screwing task under controlled laboratory conditions. In review of literature, exoskeleton efficacy is performed by focusing on muscle activity analysis using surface electromyography signals (sEMG) and a kinematic procedure acquired by different technologies. The use of wearable inertial measurement units (IMUs) and marker based optoelectronic systems is widely present in literature [4]. In recent years, newly developed markerless capture methods have been reported to process kinematic joint angles [5]. This video-based system allows the acquisition of data from cameras with the application of a dedicated software to extract joint center locations by using human pose estimation algorithm [4]. At this regard, the CapturyStudio (The Captury GmbH) software is considered in this study as a newly technique requiring a validation procedure to assess the exchangeability with the reference IMU-based method by performing a kinematic analysis over upper limb joint angles. The videos used in motion capture system (Captury) validation were acquired by BTS-EVO2 cameras (BTS Bioengineering) set in a markerless configuration and connected to the EVO Capture software used to facilitate the acquisition, visualization and post-processing of collected data. Moreover, the efficacy of MATE-XT (S.p.A. COMAU) exoskeleton is performed through kinematic analysis using IMU system (Xsens) and a muscle activity analysis related to BTS sEMG sensors (BTS Bioengineering), based on chloride (Ag/AgCl) surface electrodes, to assess respectively the joint angle changes and the occurrence of muscle fatigue between the condition while wearing the exoskeleton (Exo) and the free one (NoExo).

2. Material and methods

Acquisitions took place in Politecnico di Milano (Lecco Campus) and involved 12 healthy subjects with an equal distribution between male and female (height: 174 (±8) cm; weight: 68 (±10) kg; age: 25(±2) years). 12 sEMG probes were attached bilaterally to muscle of interest in the positions illustrated by Figure 2.1, namely right and left deltoideus anterior (RDA, LDA), deltoideus posterior (RDP, LDP), extensor carpi radialis (RER, LER), flexor carpi radialis (RFR, LFR), erector spinae (RES, LES) and rectus abdominis (RRA, LRA). Probes acquired muscle electromyographic signals and transmitted data by wireless connection to EVO Capture software that allowed the synchronization between sEMG data with the acquired videos. Subsequently, corresponding maximum voluntary contractions (MVC) were performed to allow the comparison between subjects after the processing phase. Furthermore, 11 IMUs (Xsens) were placed on the subject upper arms, trunk and head, as shown in Figure 2.1, to reconstruct kinematic angles.

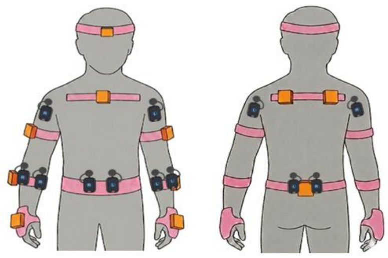

Figure 2.1: IMU (Xsens) and EMG placement

Each IMU sensor (Xsens) has an internal three-dimensional accelerometer, gyroscope and magnetometer utilizing data fusion to reconstruct body segment kinematics after the MT Software Suite software processing. Eight BTS-EVO2 cameras in markerless configuration were used to acquire the videos analysed by CapturyStudio software that can process videos coming from multiple cameras and automatically track the human movement by describing the joint angle positions of the subject after an initial correspondence between the virtual model and the human figure. The subjects were required to perform a repetitive overhead task in both Exo and NoExo conditions. The overall duration of each task was set at 10 minutes with 5 repetitions for minute corresponding to an OCRA index, an indicator of risk level, of 2.92 ranging in the very low risk classification. Each action time was indicated by a chronometer. The protocol required the subject to stand in front of the working station, whose disposition with relative height is shown in Figure 2.2, in an initial pose with both arms along the trunk.

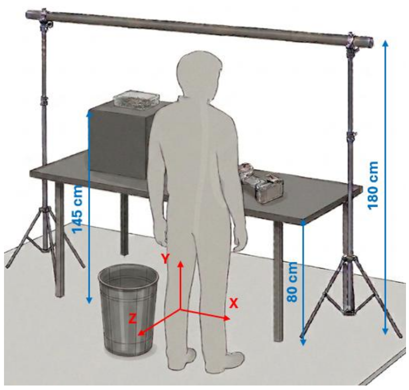

Figure 2.2: workstation set-up

At the acoustic signal, the subject was required to reach with the right hand the screwdriver placed on the table and with the left hand grasp a screw. Both tools were subsequently placed on the board, and the screwing was mimic for 5 seconds. Finally,

the subject returned to the initial posture by posing the screwdriver on the table and throwing the screw in the bin near the left leg. Between the execution of the two tasks, an acceptable amount of time (around two hours) was considered to avoid possible fatigue effects.
After the acquisition, a post processing was performed. sEMG signals were filtered with two 2nd order Butterworth filters to allow a more comprehensible analysis. Moreover, to allow the comparison between subjects all signals were normalized over the corresponding MVC value. IMU (Xsens) signals were filtered by MT Software Suite and the joint angles computation followed a ZXY Euler convention providing frame-by-frame data samples at a frequency of 60 Hz. Conversely, raw motion capture system (Captury) joint angles were acquired at 30 Hz and required a filtering process with a 4th order Butterworth filter to improve smoothness and mitigate high frequency peaks. To compare results for joint angle positions obtained by IMU system (Xsens) and motion capture system (Captury), the latter were upsampled and mapped to a matching 60 Hz frequency with a subsequent synchronization procedure. For both kinematic and muscle activation analysis, the signals were divided into cycles by detecting the starting and end point of each action. The muscles of the upper limbs and trunk were considered, while for the kinematic analysis joint angles like shoulder and elbow flexion-extension (RSfe, LSfe, REfe, LEfe) and shoulder adduction-abduction (RSaa, LSaa) were analysed. A descriptive analysis was performed by computing the mean and standard deviations values over each frame between all subjects and cycles for all acquired signals. Among the different types of indices computed, great importance is shown in Range Of Motion (ROM) and Mean Angle (MA) related to the kinematic analysis, while for the muscle activation analysis imaging sEMG (iEMG), Maximum Acceptable Effort (MAE) and Maximum Voluntary Contraction percentage (MVC%) related to the changes in Duty Cycle (DC) were considered for the time domain. Regarding the frequency domain, two additional indices were analysed: Mean Number Frequency (MNF) and Median Power Frequency (MPF). Subsequently, an inferential statistical analysis was performed to assess the statistical significance difference or parameters over all indices. An initial Shapiro-Wilk test was performed to assess normal distribution of dataset in case of p-value greater than a given threshold (α = 0.05). The elimination of outliers took place following the range interquartile method (IQR) followed by a second application of the previous normality test. Regarding the muscle activation analysis, a Box-Cox transformation was used to obtain a normal distribution of data required to perform a two-way ANOVA test to assess the presence of statistically significant different values (p-value $< \alpha$). A post-hoc pairwise Tukey analysis was used to identify the groups where this difference was observed. Finally, the actual difference among groups was assessed from the sample values before the Box-Cox transformation. Moving to the kinematic analysis, a Wilcoxon Rank-Sum test was applied to defined significant differences (p-value< 0.05). Subsequently, Spearman's Rank Correlation method was used to define the correlated coefficient ρ to evaluate a monotonic relationship between two datasets. Finally, a Bland-Altmann method was used to graphically observe the presence of a systematic bias and limit of agreement to observe the error dispersion.

3. Results

3.1 Exoskeleton evaluation

Starting from the kinematic analysis, the mean values of right and left shoulder flexion-extension angle were computed, as shown in Figure 3.1.1 and Figure 3.1.2, respectively. These mean joint angles are obtained as the average between all subjects of the mean computed over each cycle. The blue lines represent the mean value of the Exo condition, while the red ones are related to NoExo condition. The shaded areas represent the relative standard deviation.

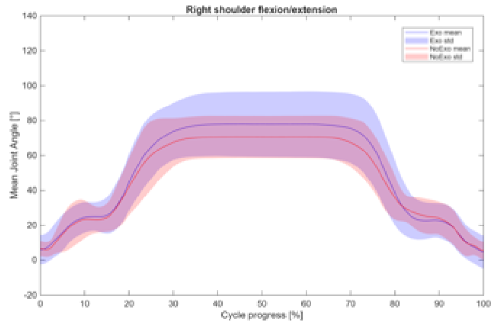

Figure 3.1.1: RSfe mean joint angle [%] over cycle progress [%]

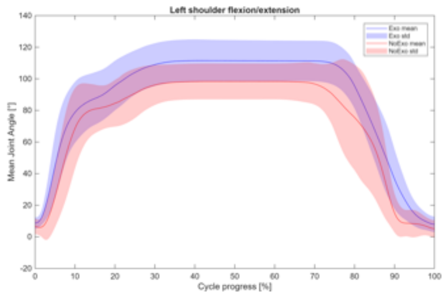

Figure 3.1.2: LSfe mean joint angle [%] over cycle progress [%]

Regarding the inferential statistics, no normal distribution of dataset was found with a Shapiro-Wilk p-value lower than α (p-value<0.05). Moreover, from two-way ANOVA test all differences among joint angle indices were found statistically meaningful except for LSfe ROM value (p-value = 0.193). Table 3.1.1 reports the actual differences between indices in Exo and NoExo condition with their relative percentage difference (%Diff.) respect to the mean value of NoExo.

Angle	Index	Exo - NoExo [°]	%Diff. [%]
RSfe	ROM	5.908	7
	MA	4.177	8
RSaa	ROM	-2.869	-13
	MA	1.056	6
REfe	ROM	-7.152	-8
	MA	-4.631	-7
LSfe	ROM	-0.725	-1
	MA	13.092	18
LSaa	ROM	-2.913	-6
	MA	4.247	19
LEfe	ROM	-12.379	-19
	MA	-3.922	-15

Table 3.1.1: Actual difference between joint angle indices in Exo and NoExo

In accordance with kinematic analysis, muscle activation didn't present normal distribution among its datasets (p-value < 0.05). Two-way ANOVA test still reported the significant differences between muscle indices in Exo and NoExo conditions whose most relevant actual difference values are shown in Table 3.1.2.

Muscle &	Index	Exo - NoExo	Exo-NoExo %Diff [%]
RDA	iEMG	-0.015	-10
RDP	iEMG	0.003	26
	DC	3.634	4
RER	iEMG	-0.009	-5
	DC	1.516	3
RFR	iEMG	-0.002	-3
	DC	2.459	3
RES	iEMG	0.005	17
	DC	4.188	5
	MNF	-	-
	MPF	1.169	1
RRA	iEMG	-	-
	DC	4.084	3
	MNF	6.252	6
	MPF	10.076	21
LDA	iEMG	0.002	6
	DC	3.078	4
LDP	iEMG	-0.003	-9
	DC	2.089	5
LER	iEMG	-0.003	-1
	DC	2.023	1
LFR	iEMG	0.001	16
	DC	1.813	1
LES	iEMG	0.009	16
	DC	4.105	6
	MNF	-1.728	-1
	MPF	-0.723	-1
LRA	iEMG	0.002	28
	DC	4.338	5
	MNF	2.256	2
	MPF	5.327	11

Table 3.1.2: Actual difference between muscle angle indices in Exo and NoExo computed only for statistically significant different groups with unit of measure in [s] for iEMG, [%] for DC and [Hz] for MNF and MPF

3.2 Motion capture system validation

In the descriptive analysis, the mean value of each joint angle across all subjects and cycles was computed to assess the general trends of IMU (Xsens) and motion capture system (Captury) acquisitions. Subsequently the statistical analysis was performed to find the statistically meaningful parameters. At this regard, normal distributions were found in LSaa ROM and LEfe MA for Exo condition in motion capture system (Captury) signal, while in IMU system (Xsens) analysis LSfe ROM, LSaa ROM and LSaa MA in EXO, RSaa ROM

and LSaa ROM in NoExo had p-value higher than α (p-value> 0.05).
Table 3.2.1 and Table 3.2.2 show the most relevant parameters observed in this section for Exo and NoExo conditions, respectively. The mean difference between motion capture system (Captury) and IMU (Xsens) acquisitions for each joint angle indices is reported. Moreover, the Wilcoxon p-values are listed and divided in statistically significant distribution (p-value<0.05) indicated by an asterisk (*) and equivalent ones. The only not significant difference was REfe ROM (p-value = 0.415). Spearman correlation coefficient ρ is reported in both tables with different gradients of color indicating the level of monotonic relationship (0.00-0.10 negligible correlation; 0.10-0.39 weak correlation; 0.40-0.69 moderate correlation; 0.70-0.89 strong correlation). Deeper is the colour gradient and higher is the level of correlation (light orange for negligible level; medium orange for weak level; deep orange for moderate level; deeper orange for strong level).

Angles		Mean Diff. [°]	p-value Wilcox.	ρ
RSfe	ROM	-23.281	0*	0.384
	MA	-26.466	0*	-0.039
RSaa	ROM	28.301	0*	-0.016
	MA	22.758	0*	0.101
REfe	ROM	-0.126	0.415	0.599
	MA	11.788	0*	0.56
LSfe	ROM	-14.985	0*	0.042
	MA	-21.452	0*	-0.135
LSaa	ROM	79.227	0*	0.295
	MA	33.814	0*	-0.028
LEfe	ROM	-6.444	0*	0.35
	MA	12.121	0*	0.633

Table 3.2.1: Mean difference, Wilcoxon p-value, correlation coefficient ρ of each combination of joint angle and indices in Exo condition

Angles		Mean Diff. [°]	p-value Wilcox.	ρ
RSfe	ROM	-13.716	0*	0.673
	MA	-24.676	0*	0.621
RSaa	ROM	14.937	0*	-0.236
	MA	14.426	0*	0.519
REfe	ROM	-8.968	0*	0.694
	MA	8.652	0*	0.662
LSfe	ROM	-5.624	0.012*	-0.119
	MA	-16.999	0*	0.261
LSaa	ROM	63.201	0*	0.34
	MA	36.913	0*	0.338
LEfe	ROM	-17.964	0*	0.191
	MA	9.656	0*	0.742

Table 3.2.2 Mean difference, Wilcoxon p-value, correlation coefficient ρ of each combination of joint angle and indices in NoExo condition

4. Discussion and conclusion

Starting with the kinematic analysis used to assess the exoskeleton effect, in Figure 3.1.1 and Figure 3.1.2 RSfe and LSfe movements show a similar trend with the NoExo condition ones. However, an increase in MA and a decrease in ROM values were observed for both shoulder joints, as shown in Table 3.1.1. This effect highlights a posture shift related to the exoskeleton's anti-gravity torque that effectively prevents the upper limbs from returning to the initial pose during the rest of the task. Moreover, a decrease in both MA and ROM values for REfe and LEfe was observed because of the shoulder MA increase coupled with a functional adaptation to the specific task constraints. Furthermore, in Table 3.1.1 a significant difference between the right and left side kinematics are described due to high asymmetry of the task and the task requirements.
Moving to the muscle activity analysis to assess the muscle fatigue level, Table 3.1.2 shows an increase of iEMG values for RES, LES and LRA muscles, while RRA remains stable, indicating a higher muscle activation due to the different distribution of loads between the exoskeleton and the subject's back counterbalanced by the activation of rectus abdominis stabilizer. This effect was enhanced by the elevated MNF and MPF values reached in RRA and LRA, paired with the stable or minor decrease in back frequencies (RES and LES) indicating a definitive postural shift. To maintain an upright trunk and counteract the backward force exerted by the exoskeleton, the subject must actively engage their abdominal core. Reducing values of iEMG for RDA, RER, RFR, LDP and LER could indicate a lower muscle activation with a consequent reduction in muscle fatigue level. However, the overall increase of DC values, with a consequent decrease in MAE and MVC%, observed in all muscles was an indicator of longer time for muscle activation related to the passive anti-gravitational torque that helps in elevating

arms while force the subject to maintain a low-level, stabilizing isometric contraction to remain steady in the initial position with both arms along the trunk.

Regarding the motion capture system (Captury) validation in comparison with the reference IMU system (Xsens), from the descriptive analysis similar trends were observed in bilateral shoulder and elbow flexion-extension in Exo and NoExo condition. However, motion capture system (Captury) overestimated the RSfe and LSfe mean joint angles, while underestimated the mean joint angles for RSfe and LSfe. Imprecisions during motion capture system (Captury) tracking procedure, related to the difficulty to assess the exact human joint position, could explain these differences. Furthermore, bilateral shoulder abduction-abduction showed a completely different mean joint angle from the reference IMU system (Xsens) in both conditions. This effect could be attributed to the spatial disposition of the cameras, which privileges the acquisition of flexion-extension movements, as well as to the intrinsic requirements of the task itself. As shown in Table 3.2.1 and in Table 3.2.2, all Wilcoxon p-values presents a statistically significant difference (p-value$< \alpha$) except for REfe ROM index (p-value = 0.415) in Exo condition. Moreover, Spearman coefficients ranged manly in negligible (0.00-0.10) or weak (0.10-0.39) monotonic relationship between the couple data enhanced by the differences between the computed ROM and MA angles that changes in magnitude from 0.126° to 79.227°. These wide discrepancies may be attributed to tracking challenges encountered during the joint alignment process.

A primary limitation of both exoskeleton evaluation and motion capture system (Captury) validation was the small number of subjects considered, which restricts the generalizability of the findings. Regarding the exoskeleton evaluation, the short task duration and the controlled laboratory environment and conditions could introduce substantial discrepancies when compared to real-world industrial settings. Moving to motion capture system (Captury) validation, limitations were observed during the tracking procedure to accurately align the digital model with the subjects' joints. Relative position of cameras and workstation, which resulted in possible occlusion of certain joints during the task could be responsible to these issues. Moreover, in this study grey scale acquisition of cameras were used. However, motion capture system (Captury) is optimized for coloured acquired videos leading to a reduction in quality detection of human joints and movements for grayscale acquisitions. Further studies are required to increase the sample size, recruiting experienced workers accustomed to overhead tasks, extending the acquisition periods and more accurately replicating industrial working environments to obtain a more comprehensive dataset to evaluate the long-term effects of the exoskeleton applied in a real working environment. Regarding the motion capture system (Captury) validation, incorporating additional cameras across multiple planes, utilizing colour video acquisition and analysing movements in different planes with wider ranges of motion could significantly enhance the tracking accuracy of the system.

References

[1] J. de Kok, P. Vroonhof, J. Snijders, G. Roullis, M. Clarke, K. Peereboom, P. van Dorst, I. Isusi, "Work-related musculoskeletal disorders: prevalence, costs and demographics in the EU," *European Agency for Safety and Health at Work,* 2019.

[2] K. H. D. Tang, "The Prevalence, Causes and Prevention of Occupational Musculoskeletal Disorders," *Global Academic Journal of Medical Sciences,* 2022.

[3] L. Botti, R. Melloni, "Occupational Exoskeletons: Understanding the Impact on Workers and Suggesting Guidelines for Practitioners and Future Research Needs," *Applied Sciences,* 14(1):84, 2024.

[4] A. E. Hurtado-Perez, M.l Toledano-Ayala, I. A. Cruz-Albarran, A. Lopez-Zúñiga, J. A. Moreno-Perez, A. Álvarez-López, J. Rodriguez-Resendiz, C. A. Perez-Ramirez, "Use of Technologies for the Acquisition and Processing Strategies for Motion Data Analysis," *Biomimetics,* 10(5):339, 2025.

[5] S. Yoon, Y. S. Li-Baboud, A. Virts, R. Bostelman, M. Shah, N. Ahmed, "Performance Evaluation of Monocular Markerless Pose Estimation Systems for Industrial Exoskeletons," *Sensors (Basel),* 25(9):2877, 2025.